ELSEVIER

Retrieval of canopy biophysical variables from bidirectional reflectance Using prior information to solve the ill-posed inverse problem

B. Combal [a,*], F. Baret [a], M. Weiss [a], A. Trubuil [b], D. Macé [b], A. Pragnère [a],
R. Myneni [c], Y. Knyazikhin [c], L. Wang [d]

[a]*INRA Bioclimatologie, Domaine St Paul, 84 914 Avignon Cedex 9, France*
[b]*Matra Marconi Space, 31 avenue des cosmonautes, 31 402 Toulouse, France*
[c]*Department of Geography, Boston University, Boston, MA, USA*
[d]*SMRI, NSMC, 46 Baishiqiao Road, Haidan District, PC 100 081, China*

Abstract

Estimation of canopy biophysical variables from remote sensing data was investigated using radiative transfer model inversion. Measurement and model uncertainties make the inverse problem ill posed, inducing difficulties and inaccuracies in the search for the solution. This study focuses on the use of prior information to reduce the uncertainties associated to the estimation of canopy biophysical variables in the radiative transfer model inversion process. For this purpose, lookup table (LUT), quasi-Newton algorithm (QNT), and neural network (NNT) inversion techniques were adapted to account for prior information. Results were evaluated over simulated reflectance data sets that allow a detailed analysis of the effect of measurement and model uncertainties. Results demonstrate that the use of prior information significantly improves canopy biophysical variables estimation. LUT and QNT are sensitive to model uncertainties. Conversely, NNT techniques are generally less accurate. However, in our conditions, its accuracy is little dependent significantly on modeling or measurement error. We also observed that bias in the reflectance measurements due to miscalibration did not impact very much the accuracy of biophysical estimation.
© 2002 Elsevier Science Inc. All rights reserved.

Keywords: Inverse problem; Prior information; Lookup table; Quasi-Newton; Neural network

1. Introduction

Remote sensing data are used to infer canopy biophysical variables, such as leaf area index (LAI), chlorophyll content (C_{ab}), daily fraction of photosynthetically active radiation (fAPAR) absorbed by the vegetation, and the cover fraction (fCover), which are involved in important physical and/or physiological processes. Radiative transfer models describing the relationship between canopy characteristics and reflectance are more and more used in the inverse mode to estimate those canopy biophysical variables from remote sensing data (Goel & Strebel, 1983; Jacquemoud & Baret, 1993; Kuusk, 1991b).

Radiative transfer model inversion consists in adjusting the values of input canopy biophysical variables $V=\{V_1, \ldots, V_{n_{var}}\}$, such as the bidirectional reflectance factors (BRFs) simulated with the radiative transfer model $\mathbf{M}$ matches the best the BRFs $\boldsymbol{R}$ measured by the sensor in a range of directions and wavebands. The model $\mathbf{M}$ requires a set of n_{var} input variables and the corresponding measurement configuration $\mathbf{C}$ (the sun illumination direction, the observation angles, and wavelengths). The model $\mathbf{M}$ matches the measured BRFs $\boldsymbol{R}$ with an error ε:

$$\boldsymbol{R} = \mathbf{M}(\mathbf{V}, \mathbf{C}) + \varepsilon \qquad (1)$$

The uncertainty ε in Eq. (1) accounts for both measurement and model uncertainties. It represents the *adequacy between the model and the measurements*. The measurement uncertainties come from the noise associated with the sensor and the data processing required to transform the sensor raw output signal into BRFs (signal digitizing, radiometric calibration, atmospheric corrections, georeferencing, etc.). Uncertainties are partly coming from inaccuracies associated to the measurement configuration variables such as directions and wavebands. The model uncertainties come

---

* Corresponding author. Tel.: +33-561-394-604; fax: +33-561-394-619.
E-mail address: bruno.combal@scot.cnes.fr (B. Combal).

from the assumptions on canopy architecture, which may not be consistent with that of the actual canopy. Further, the computation of the radiative transfer requires generally some approximations yielding in additional uncertainties in model simulations. At that time, very little work is published about the role of measurement and model uncertainties on the accuracy of canopy biophysical estimates.

Eq. (1) defines the "direct problem." Conceptually, the resolution of the inverse problem consists in finding an estimate $\hat{\mathbf{V}}$ of the variables $\mathbf{V}$ from the measured radiation $\boldsymbol{R}$.

The most popular algorithms to solve the inverse problem are the minimization algorithms, the lookup tables (LUT), and the neural networks (NNT). The feasibility of inverting radiative transfer models have been shown in many studies (Goel & Strebel, 1983; Jacquemoud & Baret, 1993; Kuusk, 1991b). Some investigations have been done to check the suitability of these algorithms to retrieve canopy variables (Knyazikhin et al., 1998, Knyazikhin, Martonchik, Myneni, Dinner, & Running, 1998; Privette et al., 1996; Weiss & Baret, 1999).

The inverse problem can be solved properly only if it is well posed, in the sense defined by Hadamard: a problem is well posed if and only if its solution exists, is unique, and depends continuously on the data (Garabedian, 1964). The problem is ill posed if at least one of these statements does not hold.

The inverse problem is by nature an ill-posed problem mainly for two reasons. Firstly, the solution of the inverse problem is not necessarily unique, but a set of solutions could lead to similar match between the measured and the simulated reflectance values (Eq. (1)). Secondly, the measurement and model uncertainties may induce large variation in the solution $\hat{\mathbf{V}}$ of the inverse problem. The error term ε (Eq. (1)) takes into account these uncertainties. Therefore, regularization techniques are necessary to obtain stable and reliable solution of the ill-posed inverse problem associated to Eq. (1).

The use of prior information is recognized as a very efficient way to solve ill-posed problems. For remote sensing applications, three different sources of prior information may be considered.

The first category of prior information corresponds to ancillary data measured on site or products provided by another sensor, e.g. leaf water content (C_{w}) estimated with radar or subpixel heterogeneity described with a high-resolution image. It could be also extended to the quantification of radiance measurement uncertainties as well as their associated structure.

The second category of prior information corresponds to the knowledge of the type of canopy architecture that defines the class of radiative transfer model to be used (turbid medium, geometric, or hybrid).

The last category of prior information concerns the knowledge of typical distribution of canopy biophysical variables used as input in radiative transfer models. This information strongly depends on the canopy type and its development stage. This prior information may be provided by an expert or by the compilation of experimental data. We should note that in the case of high spatial resolution remote sensing applications, knowledge of the canopy type and associated species is generally possible. This helps considerably in refining the prior information on canopy biophysical variables typical distribution.

In this paper, the principle of including prior information to solve the inverse problem is presented. Its implementation is particular to each inversion algorithm.

Three algorithms to solve the inverse problem are considered. Two of these algorithms, the LUT and the quasi-Newton algorithm (QNT), search for the set of canopy variables values leading to the closest match between model simulations and radiance measurements. The third algorithm is based on the training of a NNT on radiative transfer model simulations. Conversely to the previous methods, it concentrates on the biophysical variable space rather than on the radiance space. Each algorithm is presented together with the way prior information is introduced. The effect of accounting for prior information when solving the inverse problem is then evaluated.

The effect of measurement and model uncertainties on the accuracy of the solution was also investigated. When retrieving model variables from a set of "actual" measurements, the modeling error is very difficult to dissociate from the measurement error. To evaluate the role played by each error terms, synthetic data sets with controlled measurement and modeling errors levels have been generated.

The canopy variables to be retrieved were the LAI and leaf C_{ab}. These are primary variables, i.e. the radiative transfer model input variables. In addition, we considered the canopy chlorophyll content ($LAI.C_{ab}$), the fAPAR, and the fCover. These are secondary variables that are derived from combination of primary variables. For sake of simplicity, the study is restricted to the top of canopy BRFs, assuming perfect atmospheric corrections.

2. Materials and methods

Four data sets have been simulated to cover a range of radiative transfer model and measurements uncertainties. We will first describe the models used and then the way we generated measurements uncertainties.

2.1. Radiative transfer models

Two radiative transfer models with very different canopy architecture representation and radiative transfer computation were considered: a turbid medium model (SAIL) and a ray tracing (PARCINOPY) model applied on a 3D description of canopy structure.

The SAIL model (Verhoef, 1984, 1985) is a 1D turbid medium radiative transfer model. The hot spot feature description was implemented according to Kuusk (Andrieu,

Table 1
Main characteristics of the canopy simulated

Experiment number	Leaves/ plant	fCover	Canopy height (m)	LAI	C_{ab}	S
1	2	0.07	0.09	0.25	30	1.4
2	8	0.36	0.41	1.64	30	1.4
3	17	0.60	1.80	3.01	30	1.4
4	19	0.85	2.20	6.25	30	1.4
5	2	0.07	0.09	0.25	50	1.4
6	5	0.20	0.20	0.86	50	1.4
7	8	0.36	0.41	1.64	50	1.4
8	17	0.48	0.82	2.34	50	1.4
9	17	0.60	1.80	3.01	50	1.4
10	5	0.85	2.20	6.25	50	1.4
11	2	0.07	0.09	0.25	70	1.4
12	8	0.36	0.41	1.64	70	1.4
13	17	0.60	1.80	3.01	70	1.4
14	5	0.85	2.20	6.25	70	1.4
15	2	0.07	0.09	0.25	50	0.6
16	8	0.36	0.41	1.64	50	0.6
17	17	0.60	1.80	3.01	50	0.6
18	5	0.85	2.20	6.25	50	0.6

The LAI includes leaves and stems. Leaf C_{ab} for the 18 scenes of the synthetic data sets. Indices 1–18 are the experiments numbers used for the *x*-axis in (Figs. 2, 4, 6, and 7).

Baret, Jacquemoud, Malthus, & Steven, 1997; Kuusk, 1991a). Three variables are used to describe canopy structure: the LAI, the average leaf angle (θ_l) of an ellipsoidal leaf angle distribution function (Campbell, 1986), and a hot spot parameter (h).

PARCINOPY (Chelle, 1997) is a 3D radiative transfer model that uses a Monte Carlo ray tracing method to compute the BRDF of the vegetation. PARCINOPY requires the canopy architecture to be represented with an ensemble of triangles. In this study, the position of the triangles was determined according to España, Baret, Chelle, Aries, and Andrieu (1998) maize dynamic canopy architecture model. It requires the following input variables: maximum number of leaf, maximum LAI value, maximum canopy height, plant stage, and plant density. Three million rays are thrown to compute the BRFs of a given scene. That results in a relative accuracy on reflectance of 2.5% due to the Monte Carlo process (España et al., 1998).

For both SAIL and PARCINOPY models, the soil is characterized by a typical Lambertian soil reflectance spectra multiplied by a brightness parameter *S*. This allows to realistically represent the influence on reflectance of roughness and moisture variation. The typical soil spectra used corresponds to the average value between actual measurement of wet and dry soil reflectance spectra.

The PROSPECT model (Fourty, Baret, Jacquemoud, Schmuck, & Verdebout, 1996; Jacquemoud & Baret, 1990) is used to describe the leaf reflectance and transmittance that are required by SAIL and PARCINOPY. The input variables of PROSPECT are the structure variable *N*, the leaf C_{ab}, the leaf C_w, and the dry matter content (C_{dm}).

The C_{dm} was related to the leaf C_w, assuming a constant relative C_w of 80%.

2.2. The synthetic data sets

Top of canopy level reflectance observed from nadir was considered in this study. The sun zenith angle was set to 45°, and no diffuse radiation was considered. The bidirectional reflectance was computed in nine wavelengths (500, 562, 630, 692, 710, 740, 795, 845, and 882 nm).

Six different development stages of a maize canopy have been considered, thanks to España model. Table 1 gives the LAI, the number of leaves per plant, the fCover, and the canopy height for the six development stages. The corresponding SAIL canopy structure variables were derived directly from this 3D architecture model. The LAI accounts for stems that were represented by half their total developed area (Lang & McMurtrie, 1992). The average leaf angle computed from the 3D structure was found equal to $\theta_l=56°$. The hot spot parameter has been adjusted by means of the bidirectional gap fraction (Baghdadi & Baret, 1997) and found equal to $h=0.1$. Eighteen experiments corresponding to combinations of the six development stages, three different levels of the leaf C_{ab} and two soil status (wet and dry), were considered.

The SAIL model was always used in the inversion process. It requires seven input variables to describe canopy, leaf, and soil characteristics: the LAI, the average leaf angle (θ_l), the hot spot parameter (h), the C_{ab}, the leaf C_w, the leaf structure parameter (N), and the soil brightness parameter (S).

To test the sensitivity of the inversion algorithms to the adequacy between simulations and measurements, four test data sets have been generated (Table 2).

Two of them were simulated with SAIL and therefore correspond to no model uncertainty. The $1D_{bs}$ data set was derived from direct SAIL reflectance simulations with addition of a 2.5% noise (normal distribution, mean value equal to 0). To account also for the problem of possible sensor calibration errors, a relative bias of 2% was finally added to the set $1D_{bs}$ to produce the $1D_{bb}$ data set. The 1D data sets $1D_{bs}$ and $1D_{bb}$ account only for measurement uncertainty (noise or noise and bias).

The two other test data sets were generated with the 3D model. They allow to evaluate the consequence of inverting a model against a data set that is not consistent with this model. The modeling error, estimated by comparing $1D_{bs}$ with $3D_{bs}$, can reach up to 23% (relative standard deviation) in the near infrared domain. This high error level is reached mainly because the maize architecture is not consistent with the SAIL turbid medium assumption. Finally, two sets generated with PARCINOPY were considered. $3D_{bs}$ has a

Table 2
Characteristics of the four databases

$1D_{bs}$	$1D_{bb}$	$3D_{bs}$	$3D_{bb}$
Noise effect	Noise+bias effects	Noise+model effects	Noise+bias+ model effects

relative noise of 2.5% resulting from the Monte Carlo process. It therefore corresponds to that of the $1D_{bs}$ data set. Then, similarly to $1D_{bb}$, a bias of 2% has been added to $3D_{bs}$ to derive the $3D_{bb}$ data set.

2.3. Algorithms to solve the inverse problem

Three algorithms were considered to solve the inverse problem: a LUT, a QNT, and a NNT.

2.3.1. Lookup table

The most simple method to solve Eq. (1) consists in computing and storing the graph of the function $\mathbf{M(V,C)}$. The configuration $\mathbf{C}$ represents the conditions of observations, i.e. wavelengths, view, and illumination geometry.

To sample the variables $\mathbf{V} = \{\mathbf{V}_1, \ldots, \mathbf{V}_{n_{var}}\}$, 280 000 values of each variable $\mathbf{V}_i$ were randomly drawn with a distribution function specific to each variable. The space of model input variables was sampled by randomly drawing values within particular distribution functions. According to Weiss, Baret, Myneni, Pragnère, and Knyazikhin (2000), 280 000 cases were considered. The distribution function for each variable was defined in order to better sample domains where the reflectance is more sensitive to the considered variable. This was achieved in a previous step by numerical experiments. Table 3 presents the distributions selected. The reflectance was computed with SAIL. In this case, no noise and bias were added. Besides the canopy reflectance, the secondary variables considered (LAI.C_{ab}, fAPAR, and fCover) have been computed for each of the 280 000 cases.

To select the solution of the inverse problem, the LUT is sorted according to a cost function, which is a simple root mean square error (RMSE):

$$\text{RMSE} = \sqrt{\frac{1}{n_{meas}} \sum_{i=1}^{n_{meas}} (R_i - R_{i,\text{LUT}})^2} \qquad (2)$$

where R_i is the BRF measured for the wavelength i and $R_{i,\text{LUT}}$ is the BRF simulated by SAIL and stored in LUT (Eq. (2)). The solution is considered as being the distribution of the set of variables providing the smallest RMSE and can be simply represented by its median value. How-

ever, for some variables (θ_1, h, and N), the distribution of the best solution is so large (Fig. 1a) that it could take any value in the range of variation of the variable (Fig. 1a). Consequently, in these conditions, the median value will represent the center of the range instead of the high-frequency values. To prevent widely spread solutions and impose already constraints by accounting for prior information, the LUT entries have been selected according to the criterion:

$$\begin{cases} \theta_1 = 60° \pm 5° \\ h = 0.15 \pm 0.1 \\ N = 1.5 \pm 0.2 \end{cases} \qquad (3)$$

This process is a simple way to input prior information in the inverse problem. The values retained in Eq. (3) have been chosen slightly different from the actual values to simulate the uncertainty associated to prior information. Following Criterion (3), the LUT reduces down to 8032 entries. For this reduced LUT, the median of the 10 best combinations was considered as the solution of the inverse problem. Fig. 1b shows that these constraints improved significantly the accuracy of all the variable of interest.

2.3.2. Quasi-Newton algorithm

One classical way for solving the inverse problem consists in searching for the maximum likelihood of the probability density function σ of the canopy variables (Tarantola, 1987):

$$\sigma\mathbf{V} \propto \exp[(\boldsymbol{R} - \boldsymbol{R}_{sim})^T \mathbf{W}^{-1}(\boldsymbol{R} - \boldsymbol{R}_{sim}) \\ + (\mathbf{V} - \mathbf{V}_{prior})^T \mathbf{C}^{-1}(\mathbf{V} - \mathbf{V}_{prior})] \qquad (4)$$

where $\boldsymbol{R}$ is the vector of the measured BRFs, $\boldsymbol{R}_{sim}$ are the corresponding simulated BRFs, and $\mathbf{W}$ is the covariance matrix of the measurements. The diagonal elements of $\mathbf{W}$ are the variance ε^2. The $\mathbf{V}_{prior}$ variables values are estimated prior to the retrieval. They correspond to the most probable variable values. The matrix $\mathbf{C}$ is the covariance matrix of the $\mathbf{V}_{prior}$ variable values.

The covariance between measurement error and prior information is generally unknown and usually ignored. The $\mathbf{W}$ and $\mathbf{C}$ matrices are therefore diagonal. Under this assumption, the maximum likelihood of the probability density function in Eq. (4) is found when the cost function $\mathbf{C}$ is minimal. C is the sum of the RMSE computed both on the radiometric measurements and on the canopy variables prior information:

$$C = \sum_{i=1}^{n_{meas}} \left(\frac{\boldsymbol{R}^i - \boldsymbol{R}^i_{sim}}{\varepsilon^i}\right)^2 + \sum_{j=1}^{n_{var}} \left(\frac{\mathbf{V}^j - \mathbf{V}^j_{prior}}{\varepsilon^i_{\mathbf{V}}}\right)^2 \qquad (5)$$

Table 3
Transformation used to generate the distribution of the variables using uniform laws applied on the transformed variables

Variables	Minimum	Maximum	Transformed variables
LAI	0	8	$e^{-\text{LAI}/2}$
θ_1	20	75	$\cos(\theta_1)$
h	0.05	1.00	e^{-3h}
C_{ab}	20	100	$e^{-C_{ab}/100}$
C_w	0.005	0.025	e^{-50C_w}
N	1.0	2.5	N
S	0.5	1.5	S

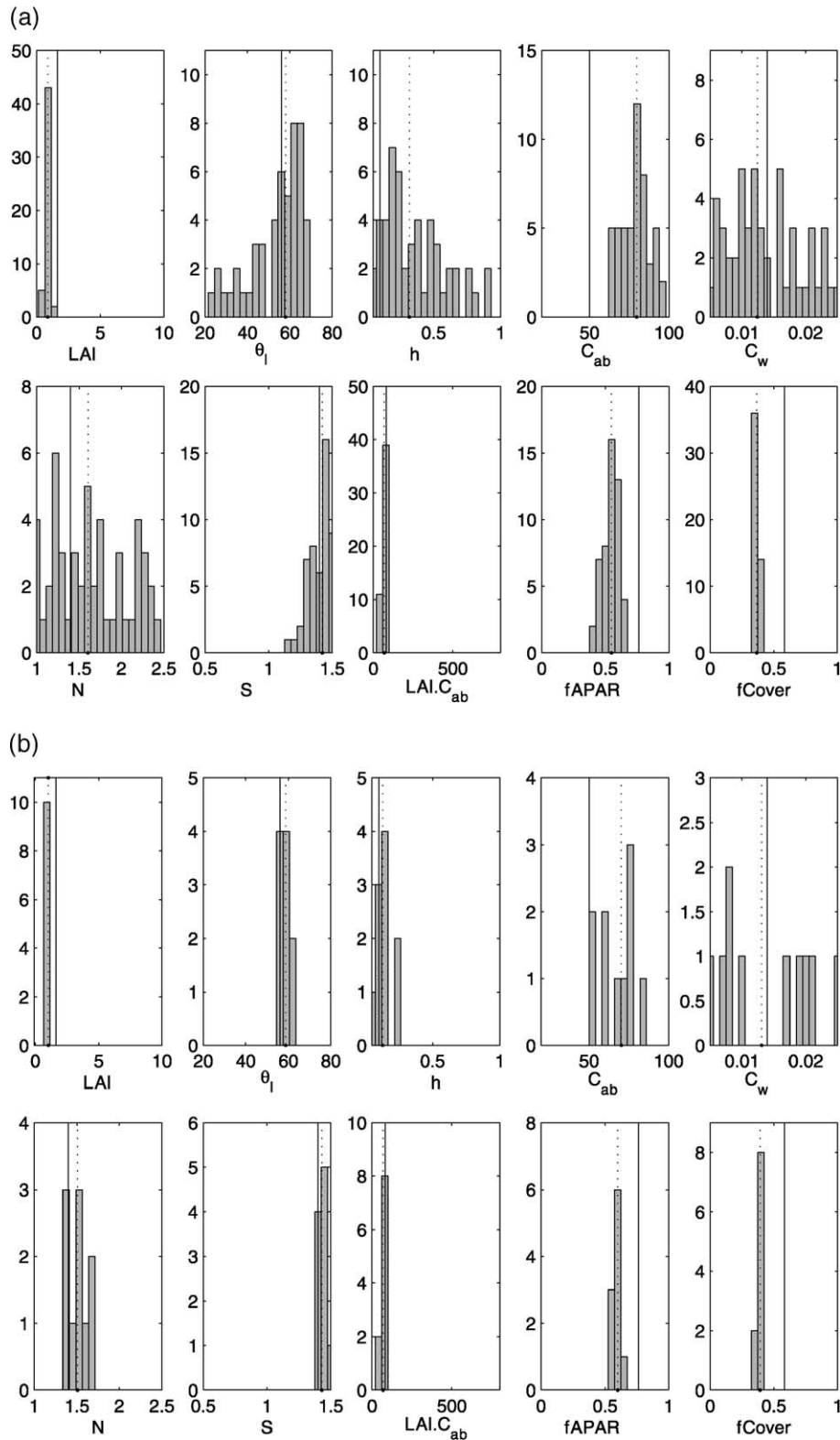Fig. 1. Distribution of the vegetation variables estimated with the LUT for Experiment 7 (see Table 1). LAI=1.64 and C_{ab}=50 µg cm^{-2} and for the dry soil (S=1.4). Results obtained on the 3D$_{bb}$ case. (a) Represents the results with the whole LUT. (b) Represents the results when some entries have been selected in the LUT according to prior information. The vertical solid line corresponds to the actual value of the variables, and the dotted line represents the median of the distributions.

Table 4
Coefficient α and prior parameter values $\mathbf{V}_{prior}$ for the QNT algorithm

Parameter	α	Prior value
LAI	.25	2
θ_l	1	60°
h	1	0.15
C_{ab}	.25	60
C_w	1	0.015
N	1	1.5
S	.25	1

where $\varepsilon_\mathbf{V}^i$ is the uncertainty associated to the prior information $\mathbf{V}_{prior}^j$ (Eq. (5)). Assessing $\varepsilon_\mathbf{V}^i$ is quite difficult, because it would require to assess the prior statistics of canopy variables $\mathbf{V}$ in the Bayesian sense. It is preferable to estimate the ratio α of the information provided by the reflectance versus the canopy variables prior information. Under the

assumption that measurement errors are proportional to the reflectance, the cost function is written as:

$$C = \sum_{i=1}^{n_{meas}} \left(\frac{\mathbf{R}^i - \mathbf{R}_{sim}^i}{\mathbf{R}^i} \right)^2 + \sum_{j=1}^{n_{var}} \left(\alpha^j \frac{\mathbf{V}^j - \mathbf{V}_{prior}^j}{\mathbf{V}_{sup}^j - \mathbf{V}_{inf}^j} \right)^2 \qquad (6)$$

The coefficients α and the prior variables values $\mathbf{V}_{prior}$ are given in Table 4. $\mathbf{V}_{inf}^j$ and $\mathbf{V}_{sup}^j$ are the lower and upper bounds for the parameter $\mathbf{V}^j$, respectively. Fig. 2 shows that if the canopy variables are retrieved only with radiometric information term in the cost function (i.e. $\alpha=0$), their estimation is inaccurate. This is a direct consequence of the fact that the inverse problem is ill posed. To overcome this problem, some prior information (the prior estimations $\mathbf{V}_{prior}$ and the coefficients α) are required. We will see in Section 3 how they were derived.
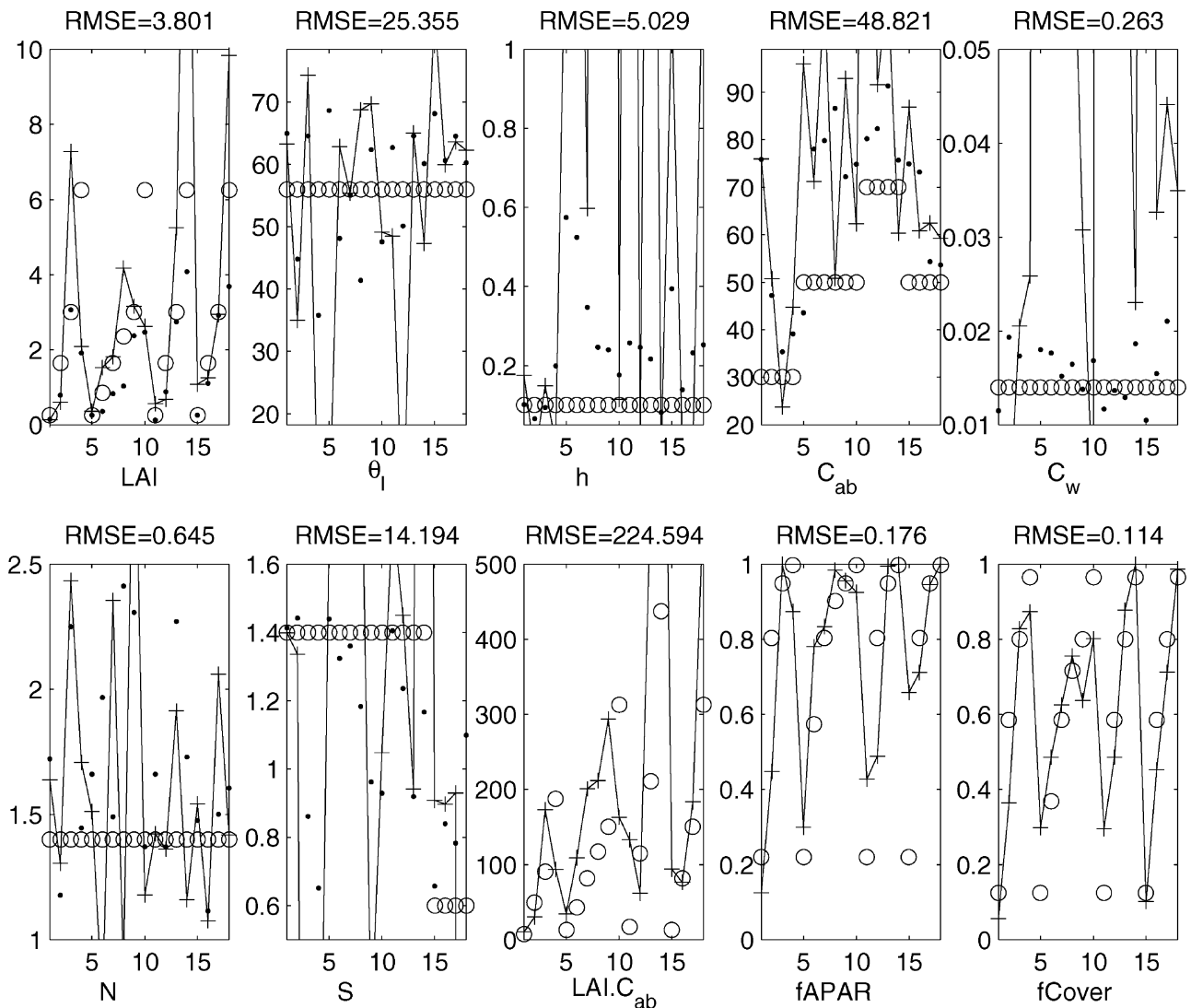

Fig. 2. Canopy variables retrieved with the QNT without constraint. Continuous line: retrieved value, dot: initial value (derived from the mini LUT), circles: actual variable value.

The QNT is widely used and allows to converge toward the minimum of the cost function very efficiently. It requires an initial value for the parameters **V** to estimates and iteratively minimizes the cost function. The initial values of the variables **V** are derived from a mini LUT (same as LUT, but with only 3000 cases). Hereafter, the term LUT_{QNT} stands for this mini LUT. Results (not shown) indicate that QNT is not too sensitive to the initial values of the initial guess derived from LUT_{QNT}.

2.3.3. Back-propagation neural network

NNTs are broadly used in remote sensing, from classification applications to inverse problem resolution(Baret, Clevers, & Steven, 1995; Buelgasim, Gopal, & Strahler, 1998; Smith, 1993). NNTs can be defined as universal tools for surface response approximation (Hornik, 1989, 1991; Leshno, Ya Lin, Pinkus, & Shocken, 1993). They enable to relate a given set of input variables to a set of output variables, irrespective to any known functional relationship between input and output, provided an implicit relationship exists between these sets. This approach is fundamentally different from LUT and QNT that require the model **M** (a functional relation between variables and BRF) to compute some cost function **C** (Eq. (6)).

Although no rigorous mathematical demonstration was provided in the literature, this approach can be understood as building the relation that transforms the BRFs measured for several wavelengths (input values) into the canopy variable values V_i (output value) (Eq. (7)):

$$G : \{ \boldsymbol{R}_1, \ldots, \boldsymbol{R}_{n_{meas}} \} \mapsto \mathbf{V}_i \qquad (7)$$

The most interesting point is that the NNT enables to account for the error terms ε (Eq. (1)).

A one-layer NNT that simulates the vegetation parameter V_i as a function of the BRFs can be written under the form:[1]

$$f \left(\mathbf{W}_i^{NNT} \times \begin{bmatrix} \boldsymbol{R}_{\lambda_1} \\ \vdots \\ \boldsymbol{R}_{\lambda_{n_{meas}}} \end{bmatrix} + \mathbf{b}_i^{NNT} \right) = \mathbf{V}_i \qquad (8)$$

where R_λ is the BRFs measured at the wavelength λ, $\mathbf{W}^{NNT}$ is the matrix of "synaptic" weight, and $\mathbf{b}^{NNT}$ is the bias added to the neurons (Demuth & Beale, 1998). The network is composed of n_1 layers of neurons. The matrix $\mathbf{W}^{NNT}$ has the dimension $n_1 \times n_{meas}$, and **b** is a vector of dimension n_1. The input (BRF) and output (**V**) values are scaled so that they fall in the range $[-1,1]$ and their mean and standard deviation are normalized. For example, the normalized BRF are computed according to $BRF_{norm}=(BRF-mean(BRF))/$ standard deviation (BRF). The neurons are arranged so that

they transform the input signal (the BRFs) into the output signal (corresponding values for a set of canopy variables). The connections between neurons are associated to a "synaptic" weight. Each neuron transforms the sum of the weighed signal from the previous neurons according to a given transfer function and a bias. In this study, the transfer functions were tangent-sigmoid and linear functions. The combination of which is recognized as capable of fitting any type of function (Demuth & Beale, 1998).

Before using NNT to retrieve the canopy variables, the network has to be trained. A training set of n_{meas} BRFs and the corresponding canopy variable values is used for this purpose. The Lavenberg–Marquardt optimization algorithm is implemented to search for the synaptic weights and neuron bias that allow the best fit with the set of canopy variables corresponding to the input BRFs in the training data set. The initial values of the weights and biases were set to a random value between -1.0 and $+1.0$.

The NNT is trained with examples extracted from the previous LUT. To improved the simulation of LAI and C_{ab}, Criterion (3) was applied to the training data set that finally contains 8032 examples. This prior information enables to estimate more accurately C_{ab}. As a matter of fact, intermediate results show that if no prior selection was introduced in the training database, the NNT was not able to correctly retrieve C_{ab}. For fAPAR and fCover, only 1000 examples, unrelated to any prior information, have been used to train the NNT. Using more examples does not improve the accuracy of the canopy variables estimation.

A 2.5% noise was added to the examples extracted from the LUT. This is a way to introduce prior information on uncertainties in the system. However, even for test data sets associated with little uncertainties, the addition of noise provides more robustness to the NNT.

The architecture of the NNT was empirically defined. Table 5 gives the architecture of the NNT as a function of the canopy variables to retrieved. The networks are here defined and trained independently for each canopy variable. Previous tests demonstrated that the concurrent estimation of several canopy variables with a single network was leading to poorer performances. These network architectures have been defined after a series of preliminary tests.

---

[1] To extent Eq. (8) to a multilayer NTT, see Demuth and Beale (1998).

Table 5
Architecture of the NNTs in function of the parameters to retrieve

Parameter	Number of neurones per layer	Transfer function	Size of the learning database
LAI or C_{ab}	6	tan-sigmoid	8032
	5	tan-sigmoid	
	3	tan-sigmoid	
	1	linear	
LAI.C_{ab}, fAPAR, or fCover	4	tan-sigmoid	1000
	1	linear	

Ten networks have been independently trained to retrieved a canopy variable, each corresponding to independent random drawing of sets of initial values of the synaptic weights and bias (Fig. 3). The median of the 10 parallel network outputs was considered as solution of the inverse problem.
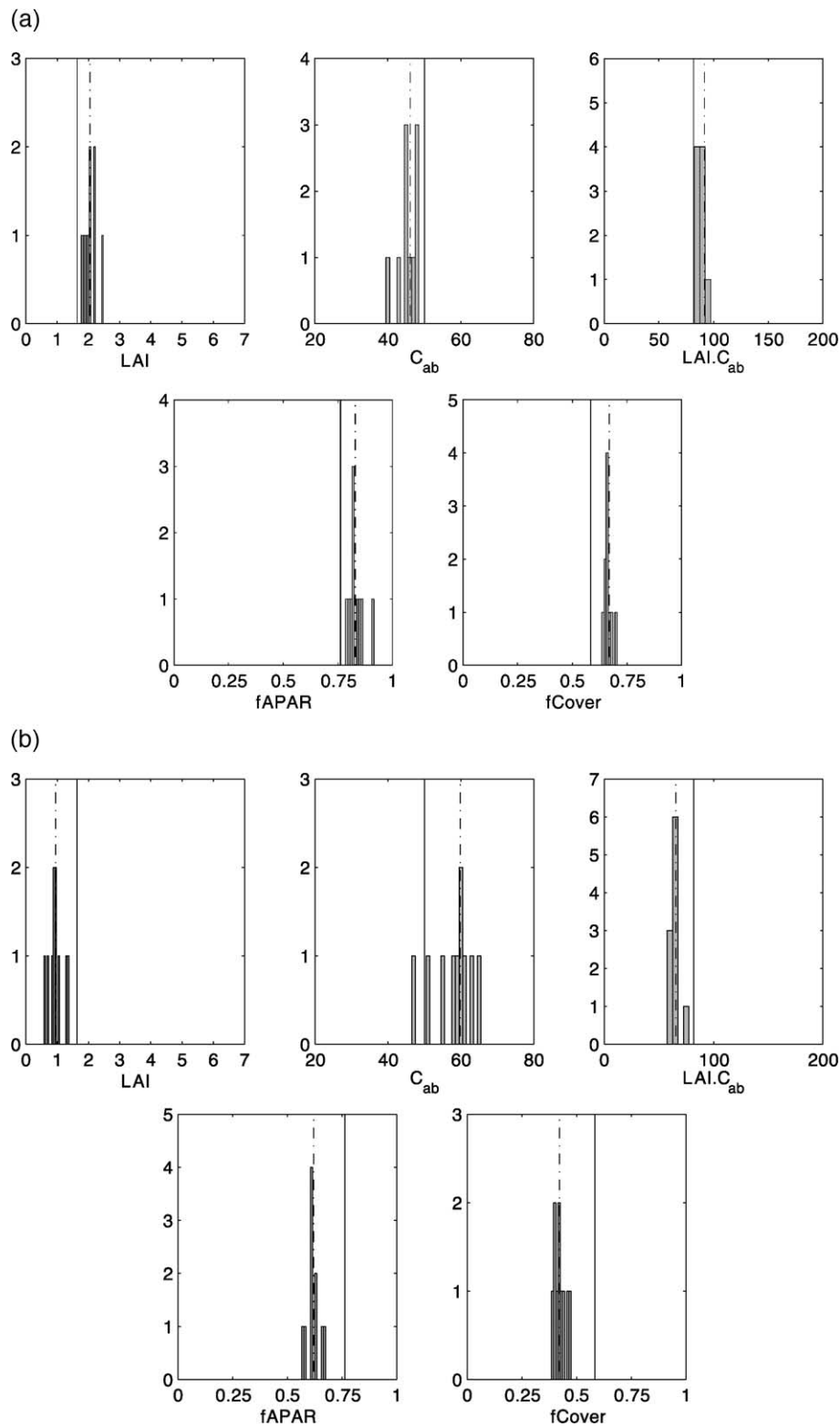

Fig. 3. Distribution of the canopy variables retrieved with the NNT for Experiment 7 (see Table 1). Vertical solid line: actual values, Dashed line: median of the distribution. (a) $1D_{bs}$, (b) $3D_{bb}$.
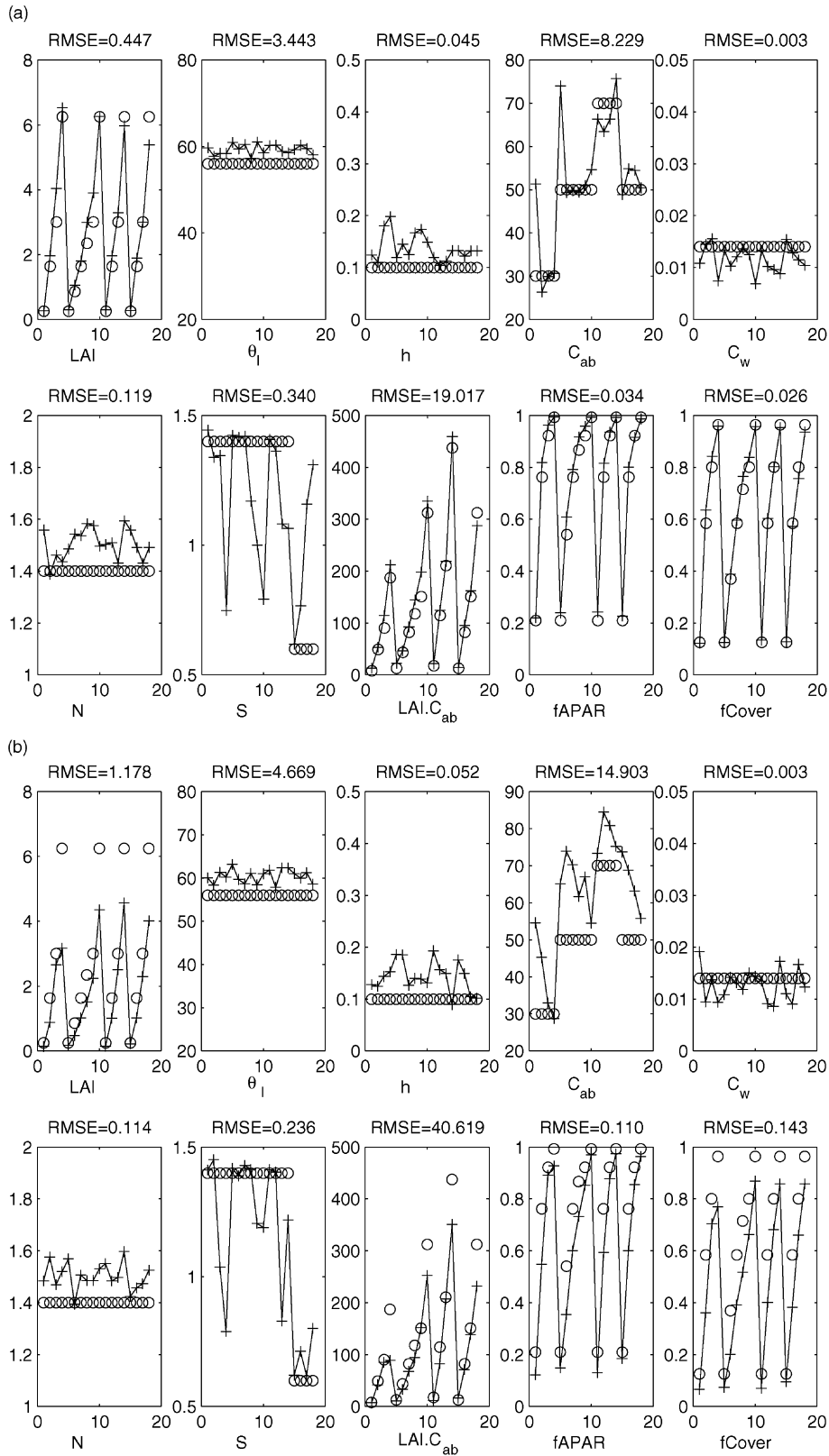
Fig. 4. Canopy variables retrieved with the LUT with prior information for the synthetic data $1D_{bs}$ (a) and $3D_{bb}$ (b). Continuous line: retrieved value, circles: actual variable value.

3. Solution of the ill-posed inverse problem

The relative RMSE (RRMSE) of the estimated canopy variables $\hat{\mathbf{V}}^i$ was used to compare the performances of the algorithms

$$\text{RRMSE}(\boldsymbol{V}^i) = \sqrt{\frac{1}{n_{\text{exp}}} \sum_{n_{\text{exp}}} \left(\frac{\hat{\mathbf{V}}^i - \mathbf{V}^i_{\text{true}}}{\mathbf{V}^i_{\text{sup}} - \mathbf{V}^i_{\text{inf}}} \right)^2} \qquad (9)$$

where $\mathbf{V}^i_{\text{true}}$ is the actual value of the canopy variable $\mathbf{V}^i$. The squared relative difference is summed for each of the $n_{\text{exp}} = 18$ experiments described in Table 1.

Results will be first inspected using the LUT algorithm, considering the effect of model and measurement uncertainties. Then, the performances of the two other algorithms will be compared. Finally, computer requirements associated to each algorithm are discussed.

3.1. Detailed results using LUT algorithm: effect of measurement and model uncertainties

The LUT enables to retrieved LAI with a relative error around 0.07 over $1D_{bs}$ and $1D_{bb}$, i.e. when no model uncertainty is considered because the 1D SAIL model used in the inverse process was also used to generate the test data sets. RRMSE dramatically increases to 0.2 when model uncertainty is considered ($3D_{bs}$ and $3D_{bb}$). Fig. 4b shows that the error on LAI comes mainly from large LAI values that are poorly estimated because of the lack of sensitivity (saturation). For the 1D cases, large LAI values are slightly overestimated (Fig. 4a), while they are underestimated over 3D cases (Fig. 4b). This confirms the observation of Combal, Oshchepkov, Sinyuk, and Isaka (2000), showing that only little information on canopy architecture is available for LAI larger than 3.

C_{ab} is retrieved with a RRMSE ≈ 0.20 for the 1D cases. RRMSE dramatically increases for the 3D cases (RRMSE>0.35). Fig. 4a shows that situations where LAI and leaf C_{ab} values are low and soil reflectance is high (Experiments 1 and 5, see Table 1), C_{ab} is overestimated. For these situations, the uncertainty about C_{ab} is particularly important because the contribution of the leaf reflectance is too weak as compared to the soil contribution.

The uncertainty on estimates of $LAI.C_{ab}$ increases from RRMSE ≈ 0.04 for the 1D cases to RRMSE ≈ 0.10 for the 3D cases. Fig. 4b shows that for large LAI (Experiments 4, 10, 14, and 18), the retrieved $LAI.C_{ab}$ value is overestimated for the 1D cases and underestimated for the 3D cases. This behavior is consistent with the previous observations on LAI.

fAPAR is retrieved accurately for the 1D cases (RRMSE ≈ 0.035). For the 3D cases, fAPAR is underestimated (Fig. 4b), and the RRMSE increases up to 0.11, which is still acceptable.

Among all the variables, fCover is the most sensitive to modeling errors. Its RRMSE depends on the model/measurement adequacy: the uncertainty increases from RRMSE
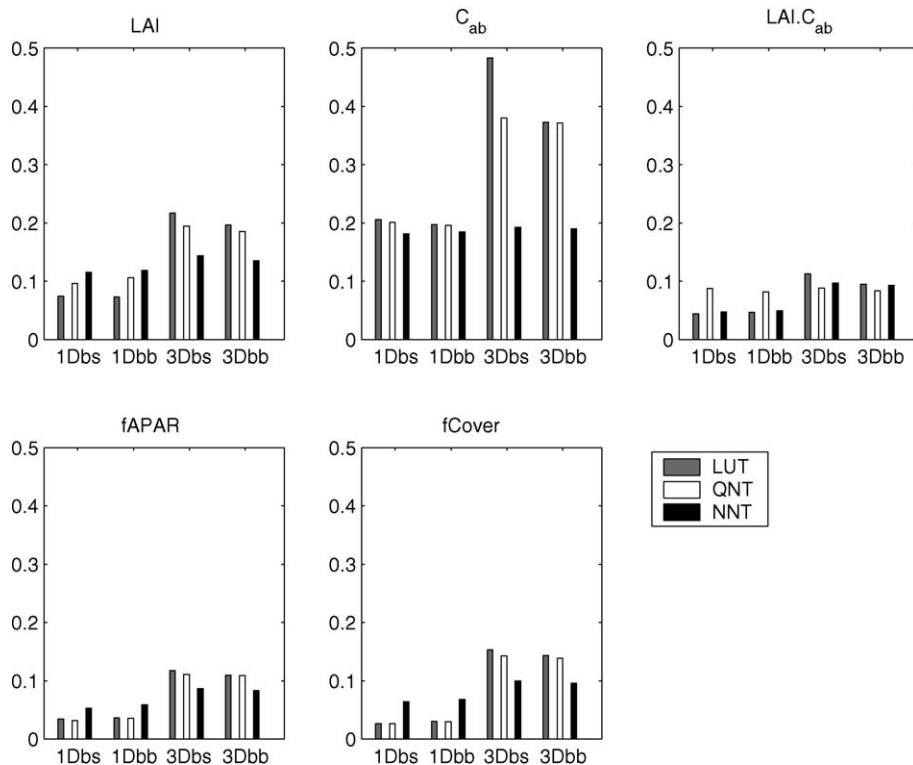

Fig. 5. RRMSE (Eq. (9)) of the LAI, C_{ab}, $LAI.C_{ab}$, fAPAR, and fCover retrieved with the LUT, the QNT, and the NNT as a function of the data sets.

≈ 0.02 ($1D_{bs}$) to RRMSE ≈ 0.15 ($3D_{bb}$), i.e. is multiplied by 7 when modeling errors are considered. The uncertainty increases dramatically for the 3D cases where SAIL does not represent properly the structure of the maize crop, as seen earlier. In consequence, fCover is slightly underestimated (Fig. 4b). However, the uncertainty of fCover for the 3D cases is slightly higher than that of fAPAR but significantly lower that on LAI C_{ab} and LAI.C_{ab} (Fig. 5).

For the cases where modeling errors are important ($3D_{bs}$ and $3D_{bb}$), the error on the retrieved variables increases significantly. This indicates that the consistency between the reflectance model and the actual canopy structure has significant consequences on the accuracy of the retrieved variables.

The leaf angle variable θ_l, the hot spot parameter h, and the leaf structure parameter N are retrieved accurately, thanks to the preselection operated on the LUT (Eq. (3)). The C_w parameters cannot be accurately retrieved because it would require some additional infrared measurements, although it was coupled here to the C_{dm} that absorbs slightly over the whole spectral domain.

3.2. Comparison with QNT and NNT algorithms

For C_{ab}, fAPAR, and fCover, the uncertainty is almost equal to that of LUT. For LAI and LAI.C_{ab}, QNT uncertainty is slightly larger than the LUT uncertainty for the 1D cases (Fig. 5). LAI, LAI.C_{ab}, and fAPAR are overestimated for the 1D cases and underestimated for 3D cases, when LAI is optically thick (LAI>3). This is again consistent with LUT observations.

For the 1D cases, NNT is less accurate than both the LUT and the QNT. This difference is due to the fact than NNT approximates the surface response defined by the learning database. The approximation leads to significant errors as compared to the two other algorithms. However, we observe that for C_{ab} and LAI.C_{ab} estimation, NNT performs similarly to the LUT.

For the 3D cases and particularly for C_{ab}, NNT is more accurate than LUT and QNT (Fig. 5). Detailed inspection of the results shows (Figs. 4b, 6b, and 7b) that some combination of variables make LUT and QNT unstable. For example, C_{ab} is largely overestimated for cases where LAI and C_{ab} have small values. In the same case (Fig. 7b), overestimation is less important with NNT.

The main advantage of the NNT on LUT and QNT is that it can be trained to retrieve only on one variable independently from the others. Another aspect is that training NNT to retrieve LAI.C_{ab} seems to be slightly more accurate than retrieving separately LAI and C_{ab} and multiplying the results. For 1D cases, RRMSE corresponding to multiplying LAI by C_{ab} is about 0.08, while RRMSE of direct estimate of LAI.C_{ab} is about 0.04.

We observe on all the cases that the effect of the bias is not very significant. This needs further investigation to understand this surprisingly small effect.

3.3. Computer resources

When applying these techniques to a large number of pixels in operational applications, computer resources may be a limiting factor. This is the reason why this issue is presented, although very little effort was dedicated to the optimization of the code used. All the computation was completed with a Sun/Solaris Ultrasparc 340 MHz/256 Mo workstation using Matlab software. In this section, we only focused on the application step, the learning step for LUT (generation of the LUT), and NNT (calibration of the synaptic weights and biases) being considered as not limiting because it is done once.

The LUT is the fastest of the three algorithms ($\approx 1.5\ 10^6$ operations s^{-1}) (Table 6) although it requires a large amount of operations because it consists in sorting a matrix. The most important point is that the computation time does not depend on the radiative transfer model used. It is computer memory and disk storage consuming. In this implementation, the full-size LUT was 28.23 MB.

When prior information is considered, the size of the LUT reduces to 8032 elements (0.81 MB) and is 35 times smaller than the full-size table. The times spent to sort this table is about 65 times shorter. For operational treatments, if prior information is known as a function of species, LUT would be both a fast and an economic approach to estimate vegetation properties.

The QNT does not require a large amount of memory. However, the time spent to find the solution is larger than the two other algorithms (Table 6). Further, it depends strongly on the radiative transfer model used because it is run at each iteration.

We observe that for the 1D case, a larger number of iterations than those of the 3D cases is required because the convergence is slower due to the "smoother" and "flatten" character of the error surface.

The NNT, although not the faster algorithm, requires the smaller number of operation to estimate canopy variables. Once the training step is achieved, only the weights are stored in files, which size is negligible. The simulation of the variables is instantaneous.

The time spent on training the NNT depends directly on its complexity. To retrieve LAI or C_{ab}, a three-layer network has been used, with six, five, and three neurons on each layers. For fAPAR and fCover, only a one-layer network with four neurons was required. In consequence, the time spend to train NNT to retrieve fAPAR or fCover is significantly smaller than for LAI or C_{ab}. However, the training step may require a long time for two reasons. Firstly, many trials are required to choose the most adequate network architecture. Secondly, each time a network has been trained, its simulations are validated against another set of examples (supervised mode). If the results are not accurate enough, the network is reinitialized, and the training sequence restarts. Consequently, the time spent on learning may be highly variable.
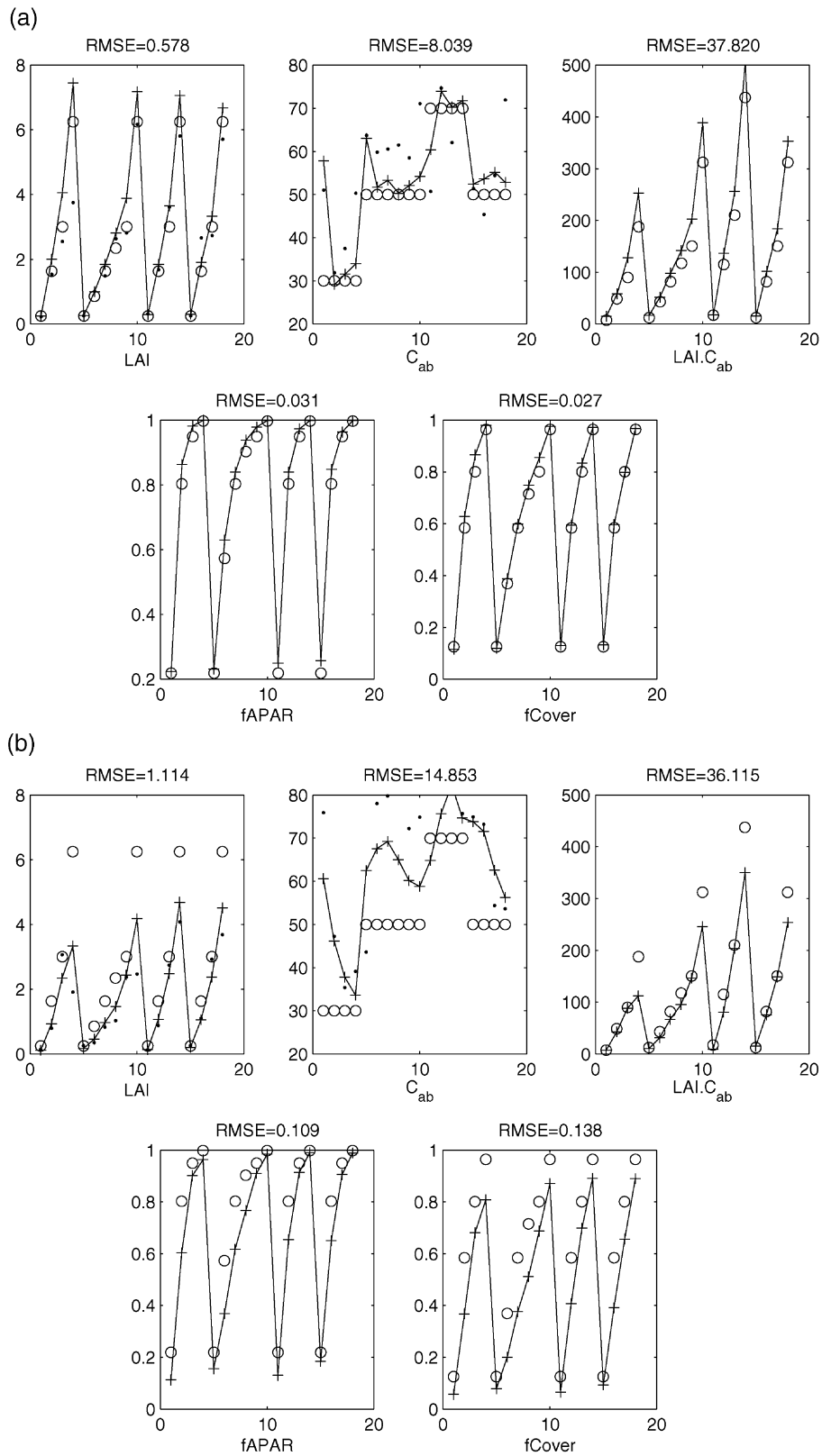
Fig. 6. Canopy variables retrieved with the QNT for the synthetic data $1D_{bs}$ (a) and $3D_{bb}$ (b). Continuous line: retrieved values, circles: actual value.
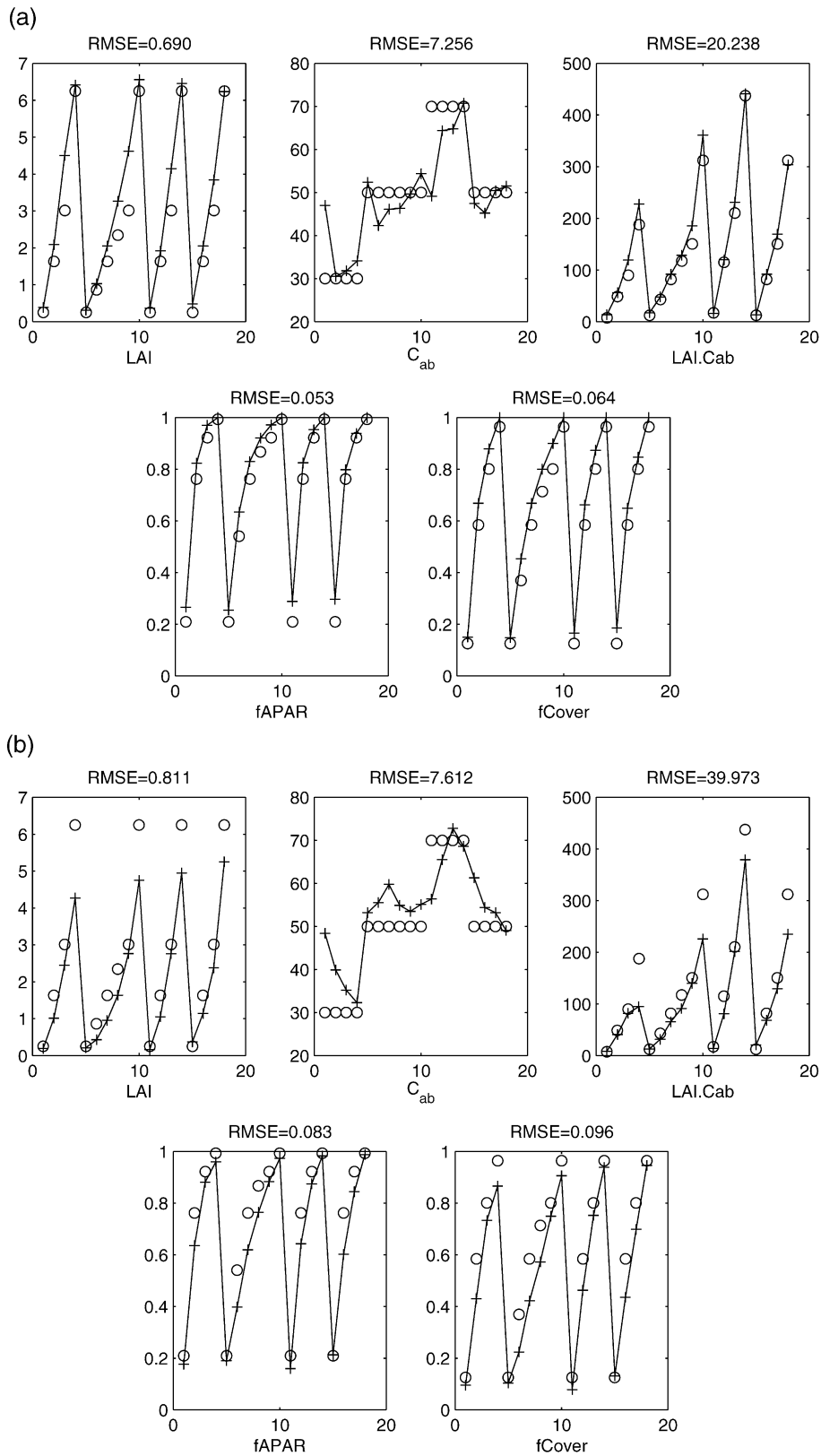
Fig. 7. Canopy variables retrieved with the NNT. (a) 1D$_{bs}$, (b) 3D$_{bb}$. Continuous line: retrieved values, circles: actual values.

Table 6
Comparison of the time and number of operations (flops) required by each algorithms to retrieve the vegetation variables for the 18 experiments

	Flops	CPU time (s)	Speed (10^6 flops s^{-1})
LUT			
8032 entries	3 192 552	2.06±0.05	1.5±0.04
280 000 entries	146 160 000	129±5	1.13±0.04
QNT			
$1D_{bs}$	123 572 011	483±4	0.25±0.02
$1D_{bb}$	116 679 471	474±9	0.25±0.04
$3D_{bs}$	90 274 896	373±3	0.24±0.02
$3D_{bb}$	84 232 104	330±6	0.25±0.05
NNT (simulation)			
LAI	269 805	2.60±0.01	0.1±0.04
C_{ab}	269 805	2.60±0.01	0.1±0.04
fAPAR	95 600	2.00±0.01	0.05±0.02
fCover	95 600	2.00±0.01	0.05±0.02

Conversely, the time spent to estimate the variables does not vary significantly with the complexity of the network. For estimation, the time required by NNT is comparable to the time required to treat LUT with prior information (Table 6).

4. Conclusion

Because of model and measurement uncertainties, radiometric information is not sufficient enough to estimate accurately the vegetation variables: some prior information is needed. Three different approaches, each one adapted to one of the three algorithms tested (LUT, QNT, and NNT), have been implemented to exploit concurrently radiometric information and prior information.

For LUT and NNT, the prior information on the distribution of the variables is represented by a selection of combination of vegetation variables among all the possible combinations. The uncertainties on measurements (and presumably models) could be introduced in the NNT by addition of noise to the learning data set. For QNT, the cost function is transformed to account for an estimate of the values of the variables and a coefficient that stands for the balance between radiometric information and prior information.

We should note that the way we included prior information into each algorithm is not unique and effort should be directed toward the evaluation of alternatives.

Besides the necessity of including prior information to overcome the limitation of the radiometric information, the present study emphasizes the role played by inconsistencies between model and measurements.

Four sets of simulated data, with a range of model and measurement uncertainties, have been used to evaluate the accuracy of the algorithms for a range of canopy variables.

LUT and QNT are very sensitive to the modeling errors. The accuracy of these algorithms depends directly on the model accuracy and on the prior information introduced. Although NNT performs poorer when only measurement uncertainties are considered, this algorithm overpasses LUT and QNT when model uncertainties are taken into account.

The present work has shown the necessity to improved the knowledge on the uncertainties related to measurements and model and its structure (dependency on wavelength, looking direction, and vegetation characteristics). To achieve this task, some efforts should be directed to the collection of data to analyze the uncertainties related to the elements involved in the radiative transfer (vegetation, soil, atmosphere, etc.) and to estimate their propagation along the remote sensing chain (sensor, digitizing, georeferencing, successive corrections, etc.). Such a description of uncertainties is required to improve the performance of the algorithms. The other important issue is to improve our knowledge on prior information about the distribution of the canopy variables used in the radiative transfer models. This could be achieved through specific experiments.

Because gathering these data will represent significant efforts that could be exploited on a range of sensors, it is necessary to define a strategy that allows a synergistic contribution and use of these experiments. The results of this preliminary and theoretical study are necessarily limited. This model inversion approach will be evaluated in the next study over actual data.

Actual measurements are required to introduce model/measurement inadequacies and realistic noise that depend on species. Validating algorithms against actual data sets will make possible to better define the balance between radiometric and prior information.

References

Andrieu, B., Baret, F., Jacquemoud, S., Malthus, T., & Steven, M. (1997). Evaluation of an improved version of SAIL model for simulating bidirectional reflectance of sugar beet canopies. *Remote Sensing of Environment*, *60*, 247–257.

Baghdadi, N., & Baret, F. (1997). *Amélioration du modèle de transfert radiatif sail à partir d'un modèle de lancer de rayons: cas du maïs*. Avignon: INRA Bioclimatologie.

Baret, F., Clevers, J., & Steven, M. (1995). The robustness of canopy gap fraction estimates from red and near infrared reflectances: a comparison of approaches. *Remote Sensing of Environment*, *54*, 141–151.

Buelgasim, A., Gopal, S., & Strahler, A. (1998). Forward and inverse modelling of canopy directional reflectance using a neural network. *International Journal of Remote Sensing*, *19*(3), 453–471.

Campbell, G. (1986). Extinction coefficients for radiation in plant canopies calculated using an ellipsoidal inclination angle distribution. *Agricultural and Forest Meteorology*, *36*, 317–321.

Chelle, M. (1997). *Développement d'un modèle de radiosité mixte pour simuler la distribution du rayonnement dans les couverts végétaux*. PhD thesis, Université de Rennes, 161 pp.

Combal, B., Oshchepkov, S., Sinyuk, A., & Isaka, H. (2000). Statistical framework of the inverse problem in the retrieval of vegetation parameters. *Agronomie*, *20*, 65–77.

Demuth, H., & Beale, M. (1998). *Neural network toolbox user's guide*. 24 Prime Park Way, Natick, MA 01760-1500: The Math Works.

España, M., Baret, F., Chelle, M., Aries, F., & Andrieu, B. (1998). A dynamic model of 3d architecture: application to the parameterisation of the clumpiness of the canopy. *Agronomie*, *18*, 609–626.

Fourty, T., Baret, F., Jacquemoud, S., Schmuck, G., & Verdebout, J. (1996). Leaf optical properties with explicit description of its biochemical composition: direct and inverse problems. *Remote Sensing of Environment*, *56*, 104–117.

Garabedian, P. (1964). *Partial differential equations*. Wiley.

Goel, N., & Strebel, D. (1983). Inversion of vegetation canopy reflectance for estimating agronomic variables: I. Problem definition and initial results using the suits model. *Remote Sensing of Environment*, *13*, 487–507.

Hornik, K. (1989). Multilayer feedforward networks are universal approximators. *Neural Networks*, *2*, 359–366.

Hornik, K. (1991). Approximation capabilities of multilayer feedforward networks. *Neural Networks*, *4*, 251–257.

Jacquemoud, S., & Baret, F. (1990). PROSPECT: a model of leaf optical properties spectra. *Remote Sensing of Environment* 34:75–91, 211.

Jacquemoud, S., & Baret, F. (1993). Estimating vegetation biophysical parameters by inversion of a reflectance model on high spectral resolution data. In C. Varlet-Grancher, R. Bonhomme, & H. Sinoquet (Eds.), *Crop structure and microclimate: characterizations and applications* (pp. 339–350). Paris, France: INRA ed.

Knyazikhin, Y., Martonchik, J., Diner, D., Myneni, R., Verstraete, M., Pinty, B., & Gobron, N. (1998). Estimation of vegetation canopy leaf area index and fraction of absorbed photosynthetically active radiation from atmosphere-corrected MISR data. *Journal of Geophysical Research*, *103*(D24), 32239–32256.

Knyazikhin, Y., Martonchik, J., Myneni, R., Diner, D., & Running, S. (1998). Synergistic algorithm for estimating vegetation canopy leaf are index and fraction of absorbed photosynthetically active radiation from MODIS and MISR data. *Journal of Geophysical Research*, *103* (D24), 32257–32276.

Kuusk, A. (1991a). The hot-spot effect in plant canopy reflectance. In R.B. Ross, & J. Ross (Eds.), *Photon–vegetation interaction* (pp. 139–159). Heidelberg: Springer-Verlag.

Kuusk, A. (1991b). The inversion of the Nilson–Kuusk canopy reflectance model, a test case. International Geoscience and Remote Sensing Symposium (IGARSS'91) (pp. 1547–1550). Helsinki (Finland): The IEEE Geoscience and Remote Sensing Society.

Lang, A., & McMurtrie, R. (1992). Total leaf areas of single trees of *Eucalyptus grandis* estimated from transmittances of the sun's beam. *Agricultural and Forest Meteorology*, *58*, 79–92.

Leshno, M., Ya Lin, V., Pinkus, A., & Shocken, S. (1993). Multilayer feedforward networks with non polynomial activation function can approximate any function. *Neural Networks*, *6*, 861–867.

Privette, J., Myneni, R., Emery, W., & Hall, F. (1996). Optimal sampling conditions for estimating grassland parameters via reflectance model inversions. *IEEE Transactions on Geoscience and Remote Sensing*, *34*(1), 272–284.

Smith, J. (1993). LAI inversion using backpropagation neural network trained with multiple scattering model. *IEEE Transactions on Geoscience and Remote Sensing*, *31*(5), 1102–1106 (ISBN: 0-444-42765-1).

Tarantola, A. (1987). *Inverse problem theory. Methods for data fitting and model parameter estimation*. The Netherlands: Elsevier Science.

Verhoef, W. (1984). Light scattering by leaf layers with application to canopy reflectance modeling: the SAIL model. *Remote Sensing of Environment*, *16*, 125–141.

Verhoef, W. (1985). Earth observation modeling based on layer scattering matrices. *Remote Sensing of Environment*, *17*, 165–178.

Weiss, M., & Baret, F. (1999). Evaluation of canopy biophysical variable retrieval performance from the accumulation of large swath satellite data. *Remote Sensing of Environment*, *70*, 293–306.

Weiss, M., Baret, F., Myneni, R., Pragnère, A., & Knyazikhin, Y. (2000). Investigation of a model inversion technique to estimate canopy biophysical variables from spectral and directional reflectance data. *Agronomie*, *20*, 3–22.